ABSTRACT

COOKSON, EDWARD JAMES. Development of the Metal Foam Electrical Resistance Heater. (Under the Direction of Dr. Albert Shih.)

This thesis presents a novel concept using a radial heating element made from porous Fe-Cr-Al metal foam in an air heater. Electrical resistance heating has been used extensively to convert the electrical energy into thermal energy. An analytic heat transfer model is first developed to estimate dimensions of the heating element. Four prototype Fe-Cr-Al metal foam electrical heaters with different levels of porosity and density are built. A more detailed computational fluid dynamics modeling of prototype heaters to include the temperature loss to the surroundings is developed. Experiments were conducted to evaluate effects of airflow rates and electrical current and measure the change of air inlet and outlet temperatures. The temperature rise in the airflow is directly proportional to electric current, and inversely proportional to the weight density of the foam. The temperature appears directly proportional to airflow rate in low density foams, while it is inversely proportional in foams of higher relative density. Experimental temperature measurements show reasonable agreement with modeling predictions. Finally, possible improvements to the initial concept are discussed.

Development of the Metal Foam Electrical Resistance Heater

by
Edward James Cookson

A thesis submitted to the Graduate Faculty of
North Carolina State University
in partial fulfillment of the
requirements for the Degree of
Master of Science

Mechanical & Aerospace Engineering

Raleigh
2003

APPROVED BY:

_____ _____

_____
Chair of Advisory Committee

Personal Biography

Edward Cookson was born in Opelika, Alabama on March of 1979, and is the son of Edward and Madeline Munn and Jim and Alison Cookson. His brother is Brian Cookson. He grew up in Gastonia, North Carolina, and attended Ashbrook High School. He graduated Magna Cum Laude with his Bachelor of Science degree in mechanical engineering from North Carolina State University in May, 2001. During his masters program he has worked as a graduate teaching assistant instructing junior undergraduate labs.

Acknowledgements

I would like to thank my graduate committee, Dr. Albert Shih of the University of Michigan, Dr. Kara Peters and Dr. John Strenkowski of North Carolina State University for their help and guidance in this project. I would also like to thank Don Floyd, Dr. Ken Butcher, and Emily Sherrill of Porvair Fuel Cell Technology in Hendersonville, NC for providing their advice and facilities for producing and testing the prototypes used during this research.

Additional thanks are due to Brian Boothe for his proofreading of the technical paper that led up to this thesis, as well as Craig Hardin and Scott Miller for taking the time to obtain the SEM images of the metal foam while at Oak Ridge National Laboratory conducting research towards their own theses.

Table of Contents

List of Figures v
List of Tables vi
1. Introduction 1
1.1. Literature Review 1
1.2. Overview of Current Research 2
2. Configuration and Material of the Metal Foam Heater 3
2.1. Design Overview 3
2.2. Foam Material 4
2.3. Brazing and Assembly of the Metal Foam Heating Element 8
3. Dimensional Design of the Metal Foam Electrical Heater 10
3.1. The Concentric Ring Model 10
3.2. Electric Resistance of a Heating Element 11
3.3. Heat Generated in the Element 12
3.4. Application of the Analytical Model 13
4. Numerical Modeling of Metal Foam Electrical Heater 16
4.1. Development of the Numerical Model 16
4.2. Numerical Modeling Results 18
5. Experimental Testing of Prototype Metal Foam Heaters 23
5.1. Experimental Design 23
5.2. Experimental Results 27
5.3. Comparison of Experimental and Numerical Analyses 32
6. Concluding Remarks 34
References 37
Appendix A. Tabulated Temperature Data for Short Duration Tests 38
Appendix B. More Detailed SEM Micrographs of Fe-Cr-Al Foams 40

List of Figures

Figure 2.1. Configuration of the metal foam electrical air heater 3
Figure 2.2. SEM micrographs of Fe-Cr-Al foams used in prototype heaters 5
Figure 2.3. Electrical resistivity measurement setup 7
Figure 2.4. Components of the metal foam heater 9
Figure 3.1. A ring segment of metal foam used in analytical and FLUENT modeling 10
Figure 4.1. FLUENT mesh of the metal foam heater. 17
Figure 4.2. FLUENT analyzed steady-state temperature profile of 100 ppi, 5 wt% density Fe-Cr-Al metal foam heating element at 50 A, 4 L/min and adiabatic outer tube wall. 19
Figure 4.3. FLUENT analyzed steady-state temperature profile at (a) 12.5mm and (b) 25.4mm from the edge of the 100 ppi, 5 wt% density Fe-Cr-Al metal foam heating element at 50 A, 4 L/min, and adiabatic outer tube wall. 20
Figure 4.4. FLUENT analyzed steady-state temperature profile of 100ppi 5 wt% density Fe-Cr-Al metal foam heating element at 50A, 4L/min, with radiation boundary condition. 21
Figure 4.5. FLUENT analyzed steady-state temperature profile at (a) 12.5mm and (b) 25.4mm from the edge of the 100 ppi, 5 wt% density Fe-Cr-Al metal foam heating element at 50 A, 4 L/min, and radiation from outer tube wall. 22
Figure 5.1. Test stand for metal foam heater experiments. 24
Figure 5.2. Close-up view of prototype heater during 20 minute testing. 25
Figure 5.3. Brooks Instrument 5850E mass flow controller used during testing. 26
Figure 5.4. Experimental temperature data for 5 hour test of 5 wt%, 100 ppi Fe-Cr-Al foam with 50 A electrical current and 4 L/min airflow rate. 27
Figure 5.5. Temperature rise of 60ppi metal foam heater after 20 minute heating time. 29
Figure 5.6. Temperature rise of 80ppi metal foam heater after 20 minute heating time. 30
Figure 5.7. Temperature rise of 100ppi metal foam heater after 20 minute heating time. 31
Figure 6.1. The cross-section of a variable thickness metal foam heating element. 35
Figure 6.2. Multi-stage heater with elements connected in series. 36

List of Tables

Table 2.1. Electrical resistivity of six Fe-Cr-Al metal foams (μΩm).....6
Table 2.2. Brazing cycle used to join the metal foam to the copper tube and rod.....8
Table 3.1. Properties of the seven ring segments used to model a 100 ppi and 5 wt% heating element.....14

1. Introduction

Electrical resistance heating is a widely used technology to convert the electrical energy to thermal energy. The resistance to electrical current in a heating element generates heat. This heat is transferred to air flowing through the heating element. This study investigates the use of open cell porous metal foam as the electrically resistant heating element.

1.1. Literature Review

An effective material for a heating element must be electrically conductive with high resistance. It also needs to be chemically stable to both oxidation and corrosion at high temperatures and have a high melting point. Commonly used electrical resistance heating materials include the iron-based alloys (Fe-Cr-Al), nickel-based alloys (Ni-Cr), carbon compounds, cermets ($MoSi_2$), silicon carbide (SiC), tungsten, molybdenum, and platinum [Hegbom, 1997; Erickson, 1995]. In this study, Fe-Cr-Al alloy, also known as Fecralloy or Kanthal, is used as the material for a metal foam heating element.

Four advantages of the porous metal foam electric resistance heater are: 1. light weight, 2. low cost, 3. adaptable to a cylindrical pipe, and 4. more uniform heating of the whole volume of air flowing through the foam. Potential applications of this heating method include household and office space heaters, particulate filtration for diesel engine exhaust after-treatment [Yoro et al., 1998], and the cleaning of airborne biological and chemical agents. When a fine mesh porous metal foam is used, this device can be employed for both filtration and heating. Such a filter can be self-cleaned by a process called regeneration,

which is accomplished by passing a high electrical current flow through the metal foam heating element to increase the temperature and burn up captured foreign particles.

1.2. Overview of Current Research

In this study, a novel concept using a radial configuration of electrical current flow is proposed. The electrical current flows through a metal foam disk, which serves as the heating element, between an outside tube and an inner center rod. The configuration, material, and manufacture of the porous metal foam heater are first presented. The analytical method to design key dimensions of the metal foam heater is discussed. Results of more detailed modeling based on computational fluid dynamics (CFD) using the FLUENT software package are presented. Finally, the experimental setup and testing results of the metal foam heating device are described and compared with modeling results.

2. Configuration and Material of the Metal Foam Heater

The following sections describe the design configuration, the metal foam material used, and the manufacture of a metal foam heater.

2.1. Design Overview

As shown in Fig. 2.1, the heating element is a thin metal foam disk inside a tube. Through the center of the metal foam disk is a cylindrical rod, which is electrically conductive and connected to the positive terminal of the DC electrical power supply. The negative (ground) terminal of the power supply is connected to the outside tube.

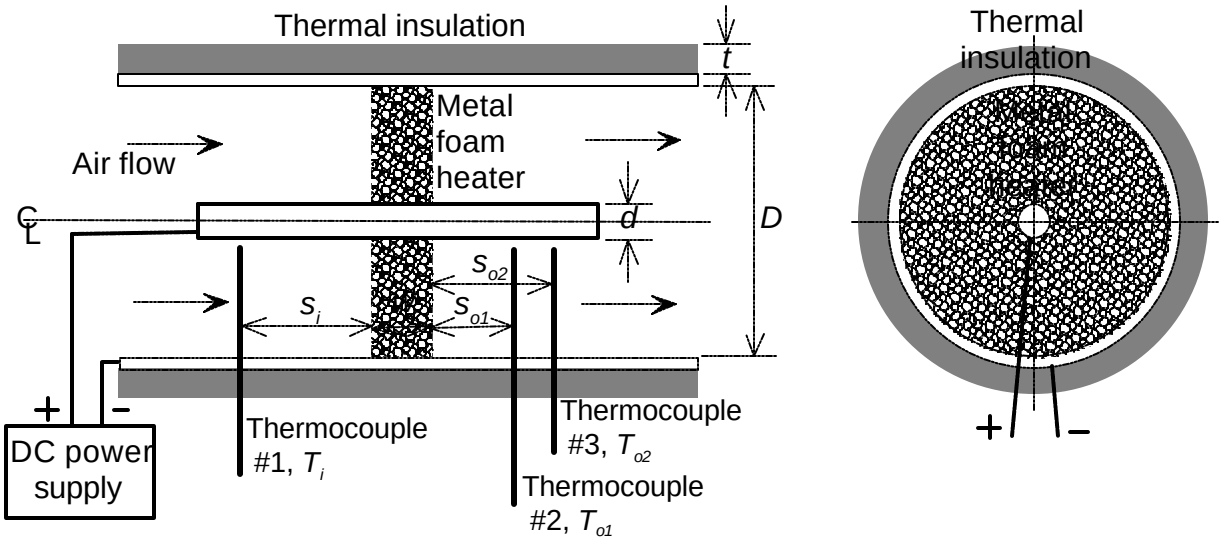

(a) Cross-section view (b) Axial view

Figure 2.1. Configuration of the metal foam electrical air heater.

Grounding the outside tube reduces the risk of electric shock if the heater is accidentally bumped while in operation. The center rod is slightly recessed into the mouth of the outer tube for the same reason. Both the tube and rod are made of copper, a highly conductive metal, so there will be little heat generation occurring in either the tube or rod. The electric current flows from the center rod to the tube through the metal foam, which is made of high resistivity Fe-Cr-Al heating element alloy. The electrical resistance generates heat, which is carried away by the air flowing through the metal foam. Temperatures of the air before and after passing the heating element are measured using K-type thermocouples, as shown in Fig. 2.1(a). One thermocouple measures the inlet air temperature, T_i, at a distance s_i from the edge of the metal foam. Two thermocouples measure the outlet air temperatures T_{o1} and T_{o2} at distance s_{o1} and s_{o2} from the other edge of the metal foam, respectively. All three thermocouples are placed close to the centerline of the tube. Outside the tube is a fiberglass thermal insulation of thickness t. The fiberglass insulation is wrapped with a layer of aluminum tape to reduce skin irritation and reduce damage to the insulation from handling the prototypes. The width of the metal foam disk is denoted as w. The inner diameter of the tube and outer diameter of the rod is designated as D and d, respectively. All size dimensions remain constant from experiment to experiment. The parameters to be designed are the relative weight density and the pore size of the metal foam used as the heating element.

2.2. Foam Material

The metal foam is made of Fe-Cr-Al alloy that can withstand operating temperatures in excess of 1200°C. The open cell foam structure, as shown in scanning electron

microscope micrographs in Fig. 2.2, consists of ligaments creating a network of inter-connected, dodecahedral-shaped cells [Lu et al., 1998]. The cells are randomly oriented and mostly uniform in size and shape.

Each ligament of the foam is hollow with a triangular-shaped hole, a result of the manufacturing technique used. The metal foams were produced using open-cell polyurethane foams as templates [Ashby et al., 2000; Banhart, 2001]. The Fe-Cr-Al alloy powder slurry with Kelzan (xanthum gum) binder was coated to the polyurethane foam and fired in a vacuum furnace. The polyurethane foam was burned out during the firing, leaving the triangular-shaped hollow hole inside each of the ligaments.

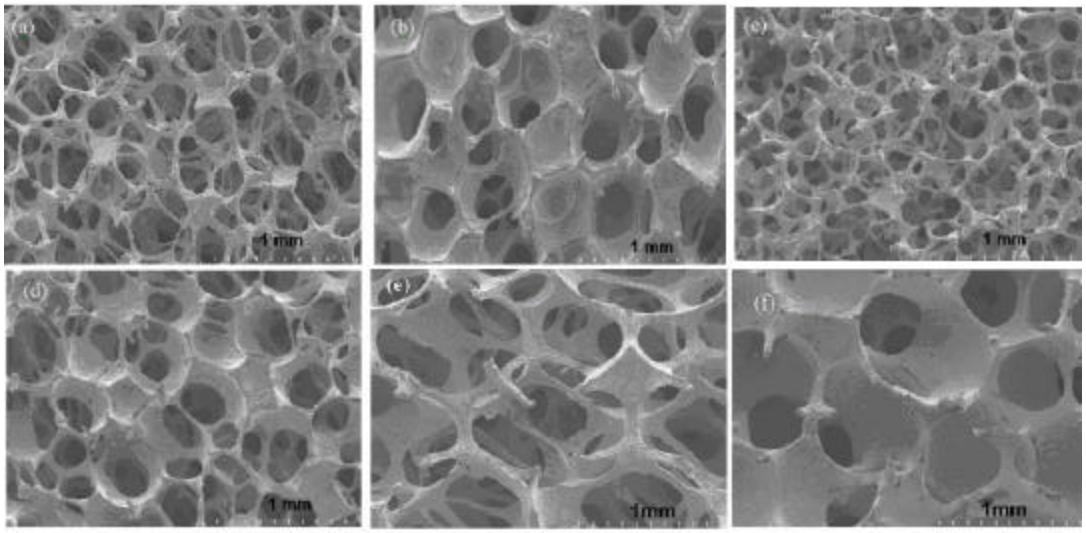

Figure 2.2. SEM micrographs of Fe-Cr-Al foams used in prototype heaters. (a) 100 ppi, 5 wt%, (b) 100 ppi, 15 wt%, (c) 80 ppi, 5 wt%, (d) 80 ppi 15 wt%, (e) 60ppi 5 wt%, and (f) 60ppi 15 wt%

Six Fe-Cr-Al metal foam heating elements with three pore sizes and two weight densities are examined in this study. Pore sizes of 60, 80, and 100 ppi (pores per inch),

which, as shown in Fig. 2.2, correspond to about 0.6 to 0.9 mm, 0.5 to 0.7 mm, and 0.4 to 0.6 mm cell size, respectively. Two levels of density are 5 and 15 wt% relative to the density of a solid Fe-Cr-Al alloy.

Bulk Fe-Cr-Al alloy has an electrical resistivity of about 1.4 μΩm [Kanthal, 2001]. In comparison, copper and 316 stainless steel have electrical resistivities of 0.017 and 0.74 μΩm, respectively. Since the metal foam is made of sintered powder, as well as highly porous, its electrical resistivity is much higher and will vary with density. Electrical resistivity was measured for each of the Fe-Cr-Al foam used for prototype heaters. The measured electrical resistivity is listed in Table 2.1.

Table 2.1. Electrical resistivity of six Fe-Cr-Al metal foams (mΩm).

Porosity	5% Density	15% Density
60 ppi	90.6	34.2
80 ppi	108	39.4
100 ppi	99.6	25.5

The electrical resistivity of each metal Fe-Cr-Al foam was determined using a foam cut from the same sample as the corresponding heating element. Direct electric current was passed through a rectangular length of foam. The voltage and current were recorded, and the resistance calculated using Ohm's law. The physical dimensions of the test specimen, length, width, and thickness, were measured. From these parameters, the resistivity was determined using Eq (2.1)

$$r = R\frac{A}{L} \tag{2.1}$$

where

A is the cross sectional area of the sample

L is the distance between the voltage probes, equivalent to the length

R is the electric resistance of sample between voltage probes.

The test apparatus for determining resistivity is shown below in Figure 2.3. Using a four point test as shown eliminates the effect of the contact resistance between the current supply leads and the foam being tested on the calculated electric resistance. The current is read directly from the power supply, and the voltage is measured from the intermediate leads with a voltmeter.

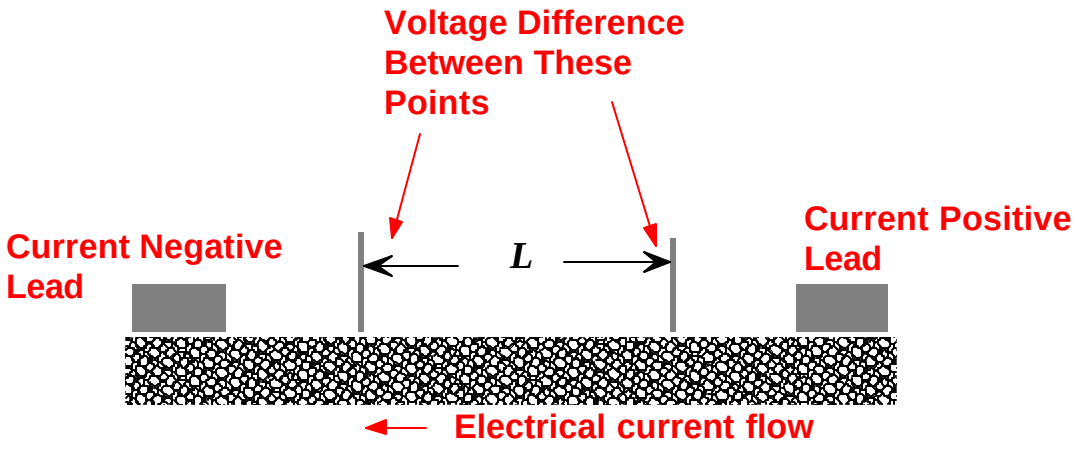

Figure 2.3. Electrical resistivity measurement setup.

The electrical resistivity of Fe-Cr-Al metal foam is much higher than the bulk Fe-Cr-Al alloy, about 20 times higher for the 15 wt% foam and 70 times higher for the 5 wt% foam. The high electrical resistance foam with 5 wt% can generate more heat per unit volume of

heat element than the 15 wt% metal foam. This will be demonstrated later in experimental temperature measurements of different metal foam heaters. There is no obvious correlation between cell size or porosity and electrical resistivity.

2.3. Brazing and Assembly of the Metal Foam Heating Element

The Fe-Cr-Al foam is brazed to the copper tube and rod. The braze paste consists of, by weight, 5 parts BNi-6 braze powder, 1 part nickel metal powder, and 1 part Kelzan binder. The BNi-6 braze, composed of Ni with 11% P and 0.1% C, is chosen because it flows freely around the joint, binds well to Fe-Cr-Al alloy, and is suitable for use at elevated temperatures. During assembly, Ni wool is used to tighten the fit between the metal foam and the inner rod and outer tube. Dummy foam elements are inserted into the ends of the prototypes without braze paste to support the rod during the handling and firing. The green prototypes are fired in a vacuum furnace using the cycle shown in Table 2.2.

Table 2.2. Brazing cycle used to join the metal foam to the copper tube and rod.

Segment	Ramp Rate (°C/min)	Set Point (°C)	Soak Time (min)
1	8	121	10
2	6	943	5
3	1.5	971	30
4	Max	871	5
5	--	Room Temp	25

Figure 2.4 shows a circular metal foam disk cut by a core drill and the brazed metal foam heater.

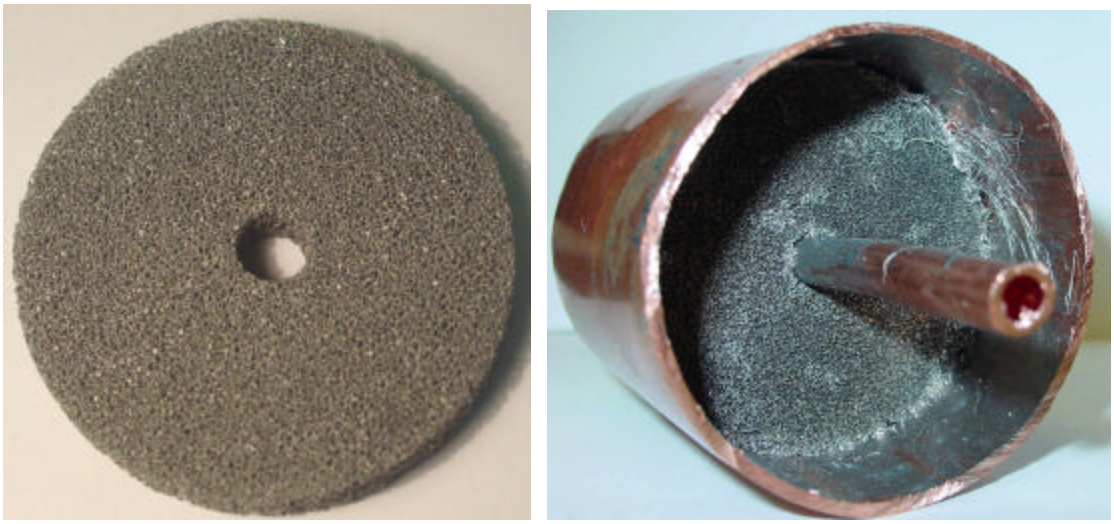

(a) (b)

Figure 2.4. Components of the metal foam heater

(a) disk metal foam heating element and (b) brazed metal foam heating device with the Ni wool on the inner surface of the outer tube.

3. Dimensional Design of the Metal Foam Electrical Heater

The analytical method is developed to design the key dimensions of the metal foam heating element and to estimate the temperature rise in the airflow.

3.1. The Concentric Ring Model

The metal foam disk is assumed to consist of a series of ring segments, as shown in Fig. 3.1. Each ring segment has the inside and outside radius of r_i and r_o, respectively, and $dr = r_o - r_i$.

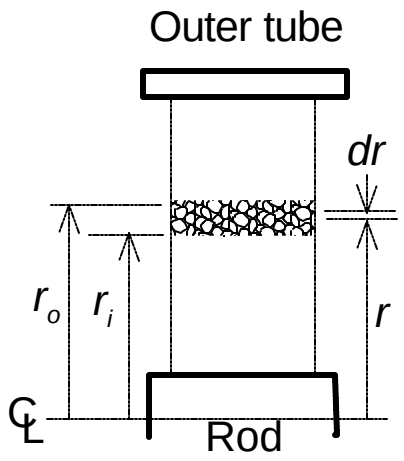

Figure 3.1. A ring segment of metal foam used in analytical and FLUENT modeling.

3.2. Electric Resistance of a Heating Element

In the metal foam disk, the electrical resistance in the radial direction of a ring cross-section with distance r from the center is designated as R. For an infinitesimal circumfrential element

$$R = r\frac{dr}{A} \tag{3.1}$$

where

r = electrical resistivity of the metal foam

$A = 2\pi rw$ is the circumfrential area of the ring cross-section

Integrating for a ring of finite thickness from r_i to r_o, the inner and outer radii of the ring respectively, the electrical resistance of the ring R_{ring} is derived as follows:

$$R_{ring} = \int_{r_i}^{r_o} r\frac{dr}{2\pi rw} = \frac{r}{2\pi w}\ln\left(\frac{r_o}{r_i}\right) \tag{3.2}$$

Since the ring segment is usually very thin, the area A of ring can be approximated by $\pi (r_o+r_i)w$ and the R_{ring} can be expressed as:

$$R_{ring} = \int_{r_i}^{r_o} r\frac{dr}{\pi (r_o + r_i)w} = \frac{r(r_o - r_i)}{\pi w(r_o + r_i)} \tag{3.3}$$

The total electrical resistance of the disk, R_{disk}, is simply the sum of the resistances of each ring.

$$R_{disk} = \sum R_{ring} \tag{3.4}$$

From the derived formulae it is noted that, for rings with constant width, the ring with larger radius has a smaller electrical resistance due to the increase in cross-sectional area allowing for the flow of electrical current. It is expected that more resistance heating and higher air temperature will therefore be generated in the inner ring segments.

3.3. Heat Generated in the Element

The total heat generated in the ring by electric resistance heating, Q_{ring}, is calculated by:

$$Q_{ring} = i^2 R_{ring} \tag{3.5}$$

Part of the heat generated is lost through the insulation to the ambient environment. For cylindrical 1-D conduction, this heat loss, Q_{loss}, is given by [Incropera and DeWitt, 2002]:

$$Q_{loss} = \frac{2p\,(T_b - T_\infty)kl}{\ln\left(\left.(r_{ins} + t_{ins})\right/ r_{ins}\right)} \tag{3.6}$$

where T_b is the temperature of the tube, T_∞ is the ambient temperature, k is the thermal conductivity of the insulation, l is the length of the cylinder, r_{ins} is the inner radius of the insulation, and t_{ins} is the thickness of the insulation. The tube has a thin wall relative to the inside diameter and is made of highly thermal conductive material. In the cross-section perpendicular to the tube center axis, temperatures at inside and outside diameters of the tube are assumed to be the same.

The bulk temperature increase, ΔT, in the airflow across the metal foam heating element can be estimated by:

$$\Delta T = \frac{Q_{gen} - Q_{loss}}{\dot{m} C_p} \tag{3.7}$$

where $\dot{m}$ is the mass flow rate and C_p is the specific heat of the air.

3.4. Application of the Analytical Model

An example is given here of a Fe-Cr-Al foam disk of w = 13 mm, inner diameter d = 6.35 mm to fit the inner rod and outside diameter D = 50.8 mm to fit inside a tube. The measured electrical resistivity of 5 wt%, 100 ppi foam is 99.6 μΩm. As listed in Table 3.1, the disk is divided into seven ring segments, each ring has radial thickness of 6.35 mm.

Table 3.1. Properties of the seven ring segments used to model a 100 ppi and 5 wt% heating element.

Ring	r_i (mm)	r_o (mm)	Electrical resistance (μΩ) [from Eq. (2)]	Electrical resistance (μΩ) [from Eq. (3)]	Heat generation rate (kW/m^3)*
1	3.18	6.35	845	813	1650
2	6.35	9.53	495	488	590
3	9.53	12.70	351	349	300
4	12.70	15.88	272	271	180
5	15.88	19.05	222	222	120
6	19.05	22.23	188	188	88
7	22.23	25.40	163	163	66

*: Based on i = 50 A and electrical resistance from Eq. (3).
Element thickness, w, is 13mm

Using Eq. (3.2), the innermost ring with r_i = 3.18 mm and r_o = 6.35 mm has an electrical resistance of 845 μΩ. For the same ring, using Eq. (3.3), a resistance of 813 μΩ is calculated. In comparison, the outermost ring with r_i = 22.23 mm and r_o = 25.40 mm, the electrical resistant calculated using both Eqs. (3.2) and (3.3) is the same, 163 μΩ. This value is significantly lower than that of the innermost ring. For the entire heating disk, summing the electrical resistance of seven ring segments yields a total electrical resistance of 2.54 mΩ using Eq. (3.2) and 2.49 mΩ using Eq. (3.3). For an electrical current i = 50 A, about 6.23 W of heat is generated in the disk Fe-Cr-Al metal foam element.

3.4.1. Analytic Results Assuming Zero Heat Loss

Using material properties of inlet air at atmospheric pressure, a temperature of 27°C, and an air flow rate of 4 L/min, results in an $\dot{m}$ of 7.74×10^{-5} kg/s, and C_p of 1007 J/kgK [Incropera and DeWitt, 2002]. Assuming the previously determined heat generation of 6.23 W, and an adiabatic boundary condition on the outer tube surface, i.e., Q_{loss} = 0, temperature rise of the air, ΔT, is 79.9°C based on Eq. (3.7). The outlet temperature therefore, is

predicted to be 107°C. This temperature rise represents an ideal case in which all electrically generated heat is carried away by the air without any loss, i.e., the outer tube is adiabatic and no heat transfer to the inner rod.

3.4.2. Analytic Results Accounting for Heat Loss

In real tests, some of the heat generated by the metal foam heater will be transferred through the outer tube, the insulation, and the inner rod to the surroundings. This section details the difficulty in accurately predicting this loss with an analytical approach.

According to the manufacturer, the thermal conductivity of the fiberglass insulation, k, is about 0.043 W/m-K. Assuming the inside radius of the insulation, r_{ins}, = 25.4 mm, a thickness, t_{ins}, = 19 mm (used in the experiment), and T_b = 107°C, T_∞ = 27°C, and l = 380 mm (the entire length of the heater pipe used in the experiment), the Q_{loss} = 15.5 W. This is higher than the 6.23 W generated by the heating element, thus it is not possible. By reducing l to 39 mm (three times the width of the metal foam) and keeping all the other variables the same, the Q_{loss} is 1.6 W. Under such Q_{loss} and using Eq. (7), the bulk temperature increase in the airflow across the metal foam heating disk is 59.5 °C, which is higher than the experimentally measured temperarure.

This example shows that using the analytical model to accurately predict the heat loss and temperature rise is difficult. More detailed computational thermal-fluid modeling and metal foam heater experiments need to be conducted to gain a better understanding of the performance of metal foam electrical heaters. These two approaches are discussed in the following sections.

4. Numerical Modeling of Metal Foam Electrical Heater

The following sections present the numerical methods used to model the metal foam heater. The results of this modeling are also discussed.

4.1. Development of the Numerical Model

The FLUENT computational fluid dynamics (CFD) software v.6.0 is used for more detailed modeling of the metal foam heater. The example analyzed in the previous section using the 50.8 mm outside diameter, 6.35 mm inside diameter, 13 mm thick, and 100 ppi, 5 wt% Fe-Cr-Al foam heating element under 50 A electrical current and 4 L/min air flow rate is modeled for mutual comparison. Using the GAMBIT preprocessor, a model consisting of seven concentric rings listed previously in Table 3 is created to represent the metal foam. Circular cross-sections of the inlet and outlet with 50.8 mm a outside diameter are also created to define a cylindrical shape control volume with the heating element inside. The 50.8 mm diameter outer surface (tube inside wall) is specified as a wall, meaning that air cannot flow through it. The distance from the inlet and outlet cross-sectional surface to the metal foam is 100 mm. This length is long enough to allow steady-state flow and temperature distributions to develop. The total length of the cylindrical control volume including inlet, foam, and outlet is 213 mm. It is noted that the inner rod is not included in the model of the inlet and outlet regions.

Figure 4.1 shows the mesh used in the analysis. The heating element is broken into seven concentric cylindrical rings, each with a uniform heat generation rate, as listed in Table 3. Meshing is done by first paving the inlet cross-section surface of the heating element, and then expanding to a volume mesh using a Cooper mesh scheme [Blacker, 1996]. Inlet and

outlet zones are then meshed using the same manner, with the heating elements surface serving as the source for mesh generation. After meshing, properties of each surface and volume of the model are assigned. Porosity is assigned to the foam sections in the FLUENT solver.

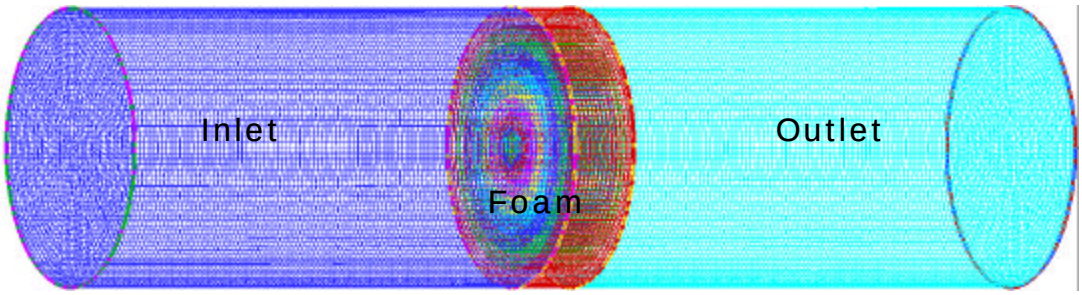

Figure 4.1. FLUENT mesh of the metal foam heater.

The outlet air is assumed to be uniform atmospheric pressure since the heater outlet is open to ambient room conditions. The inlet cross-section is specified with a uniform velocity, V_{in}, which can be varied to correspond with the mean velocity of different flow rates by assuming uniform flow.

Three parameters, viscous resistance (R_{visc}), inertial resistance (R_{iner}), and porosity, are required in FLUENT to specify for the porous region of the metal foam heater. The viscous and inertial resistances for the metal foam with air as the working fluid have been tested at Porvair [Floyd, 2001].

$$R_{visc} = 745400 r_w^{2.06} e^{0.0364 p^{0.63}} \tag{4.1}$$

$$R_{iner} = 7.44 r_w^{2.06} p^{0.63} \quad (4.2)$$

where r_w is the percentage of weight density and p is the porosity of the foam in pores per inch (ppi). For FLUENT, the porosity input is $1-r_w$. For example, the 5 wt% dense metal foam has the porosity input of 0.95.

4.2. Numerical Modeling Results

4.2.1. Results of Numerical Modeling with Adiabatic Wall Condition

The outer wall of the heater was initially modeled as adiabatic insulation (zero heat flux). Results of temperature profiles for the 100 ppi, 5 wt% Fe-Cr-Al metal foam under 50 A electrical current heating, and 4 L/min air flow rate are shown in Fig. 4.2. In the inlet, the temperature is uniform at 27°C. In the metal foam, for inner ring segments, high temperatures in the 114 to 124°C range can be seen inside the metal foam disk. On the outside rings of the foam disk, the temperature drops to about 75 to 85°C. In the outlet section, the air temperature ranges from 85°C near the outside tube to 95°C near the center axis. This number matches well with the 107.0°C of the uniform outlet temperature estimated in the analytical model.

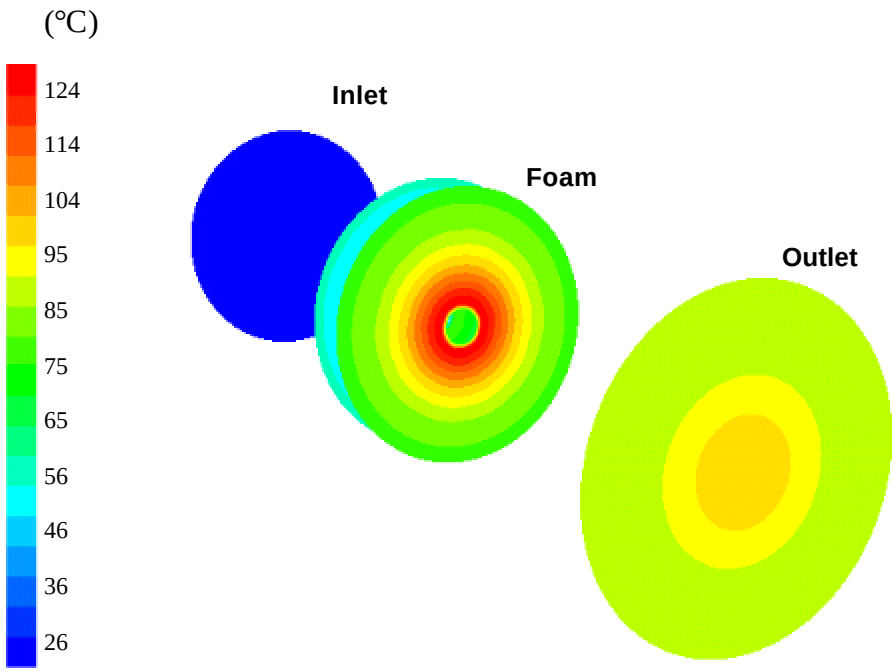

Figure 4.2. FLUENT analyzed steady-state temperature profile of 100 ppi, 5 wt% density Fe-Cr-Al metal foam heating element at 50 A, 4 L/min and adiabatic outer tube wall.

Figure 4.3 shows two cross-sections of the temperature contours at a distance of 12.5 mm and 25.4 mm from the edge of the metal foam heater. For the cross-section close to the metal foam, as shown in Fig. 4.3(a), high temperature gradient with 118°C in the center to 75°C near the outside tube can be seen. The fluid mixed and heat was transferred during the next 12.5 mm of travel. As shown in Fig. 4.3(b), more uniform temperature distribution with 112°C in the center and 69°C near the outer tube can be observed.

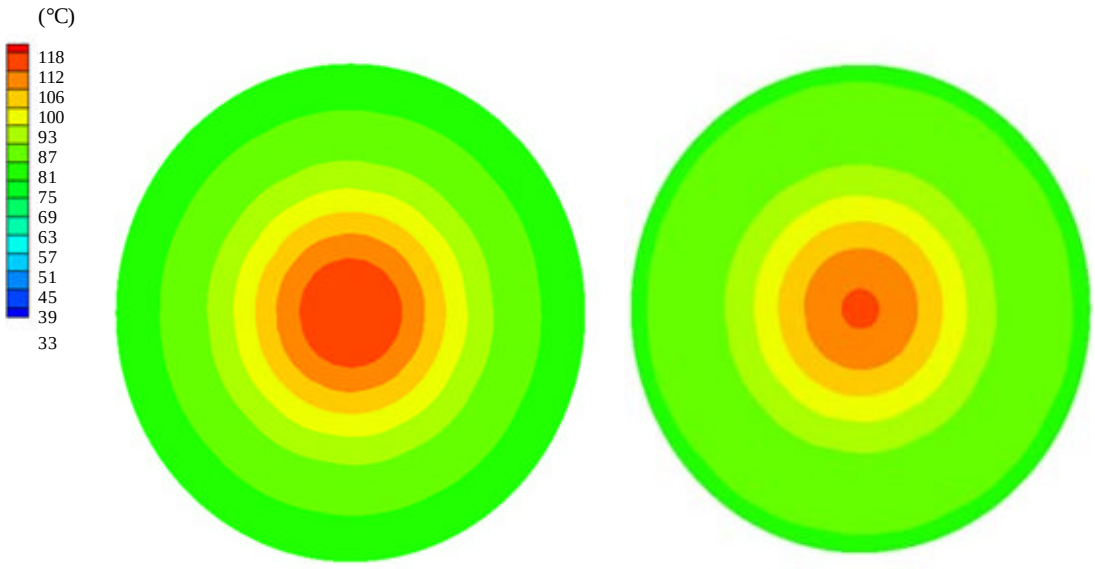

Figure 4.3. FLUENT analyzed steady-state temperature profile at (a) 12.5mm and (b) 25.4mm from the edge of the 100 ppi, 5 wt% density Fe-Cr-Al metal foam heating element at 50 A, 4 L/min, and adiabatic outer tube wall.

4.2.2. Results of Numerical Modeling with Radiation from Wall Condition

The insulation on the actual prototype is not effective enough for the outer wall to be considered adiabatic. In order to make the model better match the experimental data, the boundary condition on the outer wall must be changed. By changing the boundary condition in the FLUENT modeling to radiation to 300 K surroundings, the temperature values predicted by the model are more consistent with experimental results. Figure 4.4 shows the inlet, outlet, and foam surface temperature profiles in the model with the radiation boundary condition. Again, the model considers 100 ppi 5 wt% Fe-Cr-Al metal foam as the heating element, with 50 A current an 4 L/min airflow as the test conditions. The inlet temperature remains uniform at 27 °C. In the metal foam, the temperature in the inner rings is between

117 °C and 108 °C, and the temperature in the outer rings is between 81 °C and 72 °C. These values are about the same as the adiabatic model. At the outlet of the model, however, the air temperature ranges from about 90 °C near the center to 27 °C near the wall. FLUENT computes the mass-weighted average temperature at the outlet to be about 40 °C.

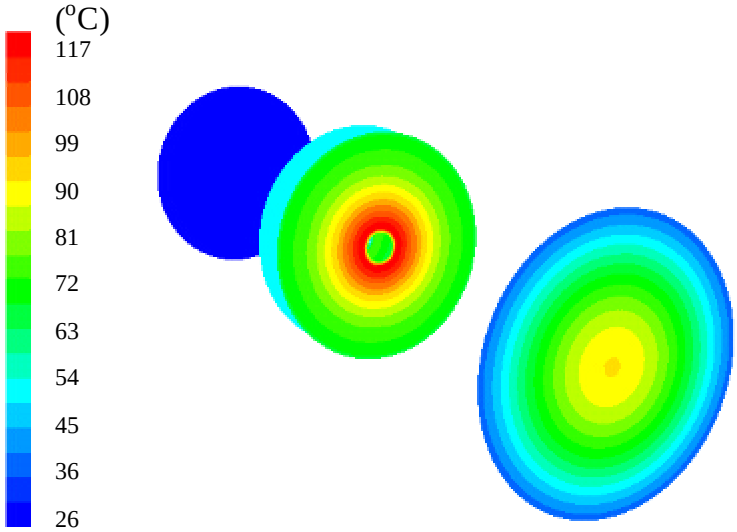

Figure 4.4. FLUENT analyzed steady-state temperature profile of 100ppi 5 wt% density Fe-Cr-Al metal foam heating element at 50A, 4L/min, with radiation boundary condition.

Figure 4.5 shows the temperature contours of two cross sections at distances of 12.5 mm and 25.4 mm from the edge of the metal foam heater. For the cross-section close to the metal foam, as shown in Fig. 4.5(a), high temperature gradient with 112°C in the center to 55°C near the outside tube can be seen. The fluid mixed and heat was lost to the surroundings while traveling from 12.5mm to 25.4mm. As shown in Fig. 4.5(b), the lower temperatures, with 100°C in the center and 44°C near the outer tube can be observed.

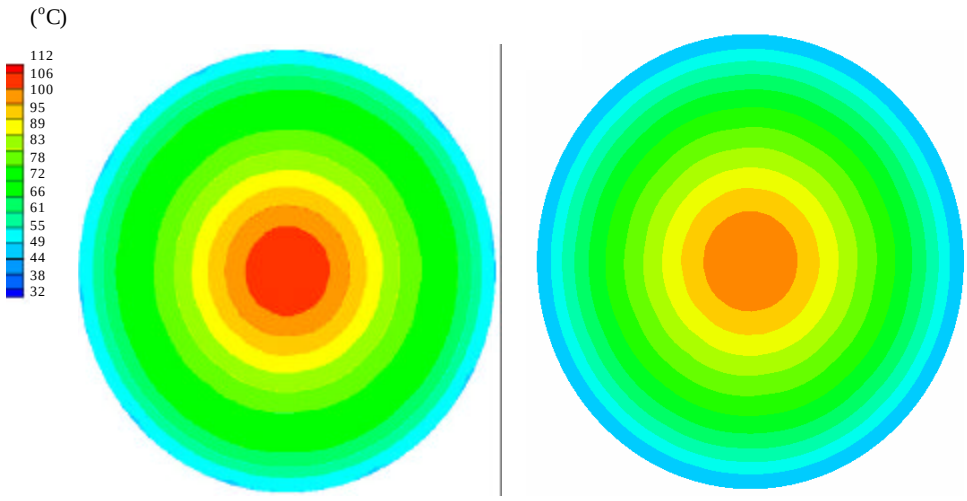

(a) (b)

Figure 4.5. FLUENT analyzed steady-state temperature profile at (a) 12.5mm and (b) 25.4mm from the edge of the 100 ppi, 5 wt% density Fe-Cr-Al metal foam heating element at 50 A, 4 L/min, and radiation from outer tube wall.

5. Experimental Testing of Prototype Metal Foam Heaters

The design of experiments for metal foam heaters, results from temperature measurement of the metal foam heater experiments, and discussion of the modeled and measured temperatures are presented.

5.1. Experimental Design

The experimental metal foam heaters, as shown in Fig. 2.3, use a standard copper tube of 50.8 mm inside diameter with a 1.5 mm wall thickness and a copper rod of 6.35 mm outside diameter. The width of the metal foam, *w*, is 13 mm. These dimensions match those used in analytical and numerical modeling. The total tube length is 380mm, with the metal foam located in the center. Outside the tube, a layer of 19 mm thick fiberglass thermal insulation was used.

As discussed in Sec. 2.2, six heating elements are made of Fe-Cr-Al metal foam with 60, 80, and 100 ppi porosity and 5 and 15% weight density. These metal foam heating elements are brazed to the copper tube and rod to make six heating devices for experiment.

The test stand used for the experiments is shown in Figure 5.1. The DC power supply in the lower-left of the figure was used to generate the desired electric current through the heating element. A mass flow controller, Brooks Instrument 5850E, was used to control the volume of air flow rate through the metal foam heating element. A differential pressure gage was connected between the inlet and atmospheric conditions in an effort to compare pressure drop through the heater at the different flow rates and foam parameters. Even with a very sensitive 0-2 inH_2O gage, no measurable pressure drop occurred. This is probably because the flow rates studied in these experiments were quite low and the heating element was thin

in the axial direction. The pressure gage was removed from later tests. The heater is mounted to the test stand panel using large U bolts.

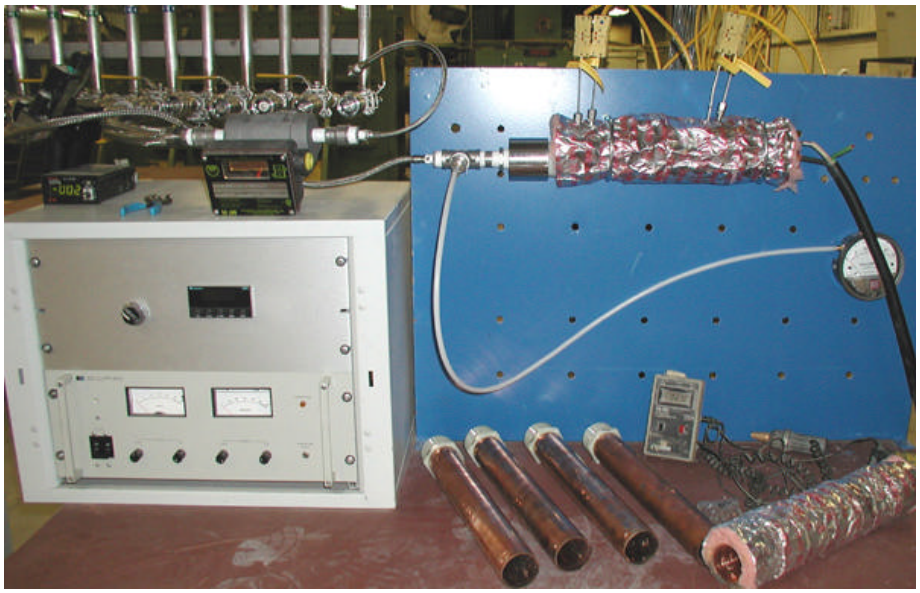

Figure 5.1. Test stand for metal foam heater experiments.

A closer view of the heater and instrumentation is shown in Figure 5.2. The pair of inlet thermocouples is pictured on the left, and the outlet pair on the right. The power supply leads can be seen attached to the right side of the heater. The black "hot" lead is simply crimped into the end of the hollow center rod. The white "ground" lead is attached to the outer tube with a sheet metal screw and a ring terminal connector. Inlet air from the mass flow controller is attached via the stainless steel coupling on the left side of the figure.

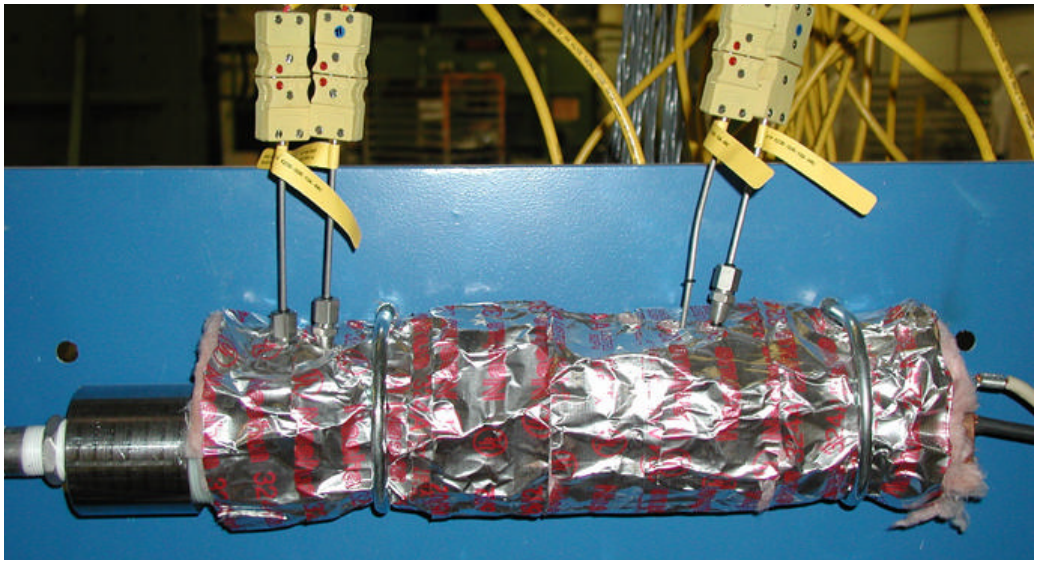

Figure 5.2. Close-up view of prototype heater during 20 minute testing.

The mass flow controller consists of two parts, a display unit and a control valve. The control valve is connected to the compressed air supply in the building by a pressure regulator, to reduce the effects of pressure variations in the line. Figure 5.3 shows the flow controller in detail.

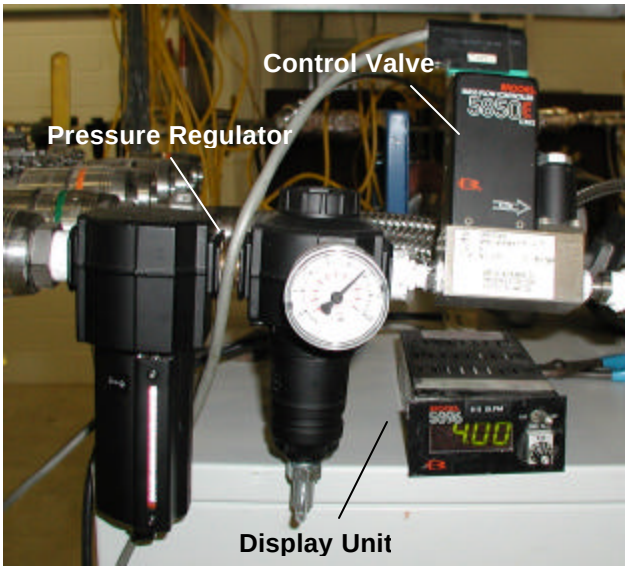

Figure 5.3. Brooks Instrument 5850E mass flow controller used during testing.

Two sets of experiment were conducted. One is the 5 hour long-duration test using the 5 wt%, 100 ppi metal foam heater to study the characteristics of the metal foam heater for an extended period of time and the time required to reach the steady-state condition. Another is a set of tests conducted on the six metal foam heaters. For each prototype, four levels of air flow rate, 0.5, 1.0, 2.0, and 4.0 L/min, and three levels of electrical current, 30, 40, and 50 A were tested. Prototype 1 was damaged while setting up the test area, so no results are available for the 60 ppi 5 wt% foam. In total, 60 experiments were conducted.

The ambient, averaged inlet, and averaged outlet temperatures were recorded during the long-duration test. This averaging is done in real-time by the data-acquisition equipment. During the short duration tests, a single inlet thermocouple is used. For some of the short experiments, the temperature on outside diameter of the tube is also recorded to determine the amount of heat lost to the surroundings (Q_{loss}).

5.2. Experimental Results

5.2.1. Steady-State Temperatures of a Foam Heater

Figure 5.4 shows the inlet, ambient, and averaged outlet air temperatures recorded for the 5 hour test.

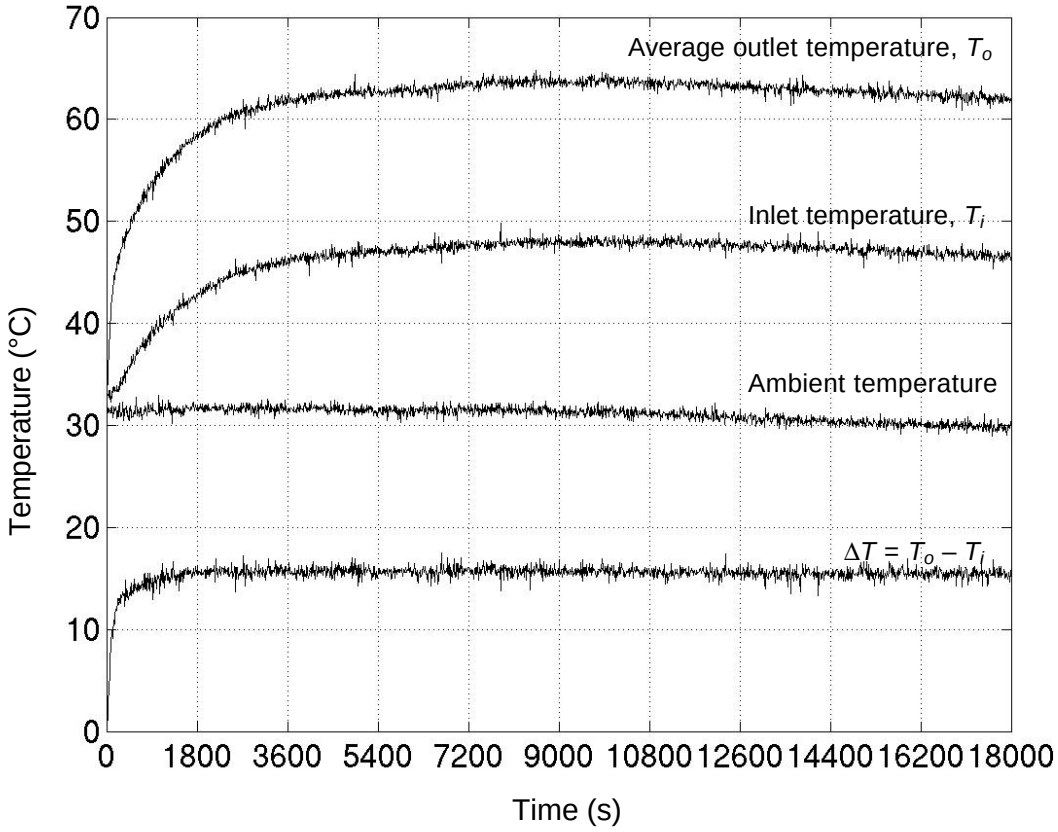

Figure 5.4. Experimental temperature data for 5 hour test of 5 wt%, 100 ppi Fe-Cr-Al foam with 50 A electrical current and 4 L/min airflow rate.

The ambient temperature starts at about 32 ℃ and gradually drops to 29 ℃ after 5 hours. All the tests were conducted in a shop floor without temperature control, which is the reason for this temperature fluctuation. The inlet temperature, T_i, gradually increased from the ambient 32 ℃ to about 47 ℃ after 3 hours (10800 sec) of testing. Following the trend of

ambient temperature, T_i slightly dropped from hour 3 to 5. The gradual increase in T_i is due to the heat conducted from the outer tube and inner rod to the front end of the heating device and pre-heat the inlet air. The average outlet temperature, T_o, also gradually increased to about 64 °C after 3 hours. The difference of outlet and inlet temperature, ΔT, is also plotted in Fig. 8. This temperature difference reached steady-states condition of about 16 °C after 20 to 30 min.

5.2.2. Effects of Air Flow Rate and Electric Current

As shown in Fig. 5.4, the outlet-inlet temperature difference after 20 min is close to the steady-state condition. Results of the temperature rise ($\Delta T = T_o - T_\infty$) of the 60 test conditions using 5 metal foam heating elements at 4 levels of air flow rate and 3 levels of electrical current flow are shown in Figures 12 through 14. The effect of electrical current, air flow rate and metal foam porosity (pore size), and wt% are studied. For 60ppi metal foam results are only available for 15 wt% foam. The temperature rises after 20 min for this prototype are shown in Figure 5.5.

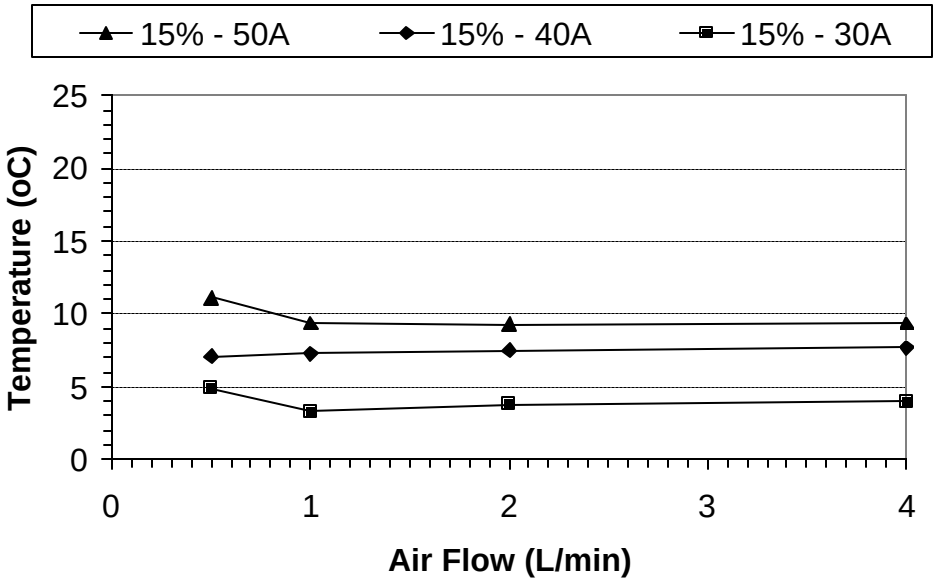

Figure 5.5. Temperature rise of 60ppi metal foam heater after 20 minute heating time.

The results for 80 ppi foam are summarized in Fig. 5.6. Here one can clearly see that the lower density foam has a much larger temperature rise at a given electric current and airflow rate.

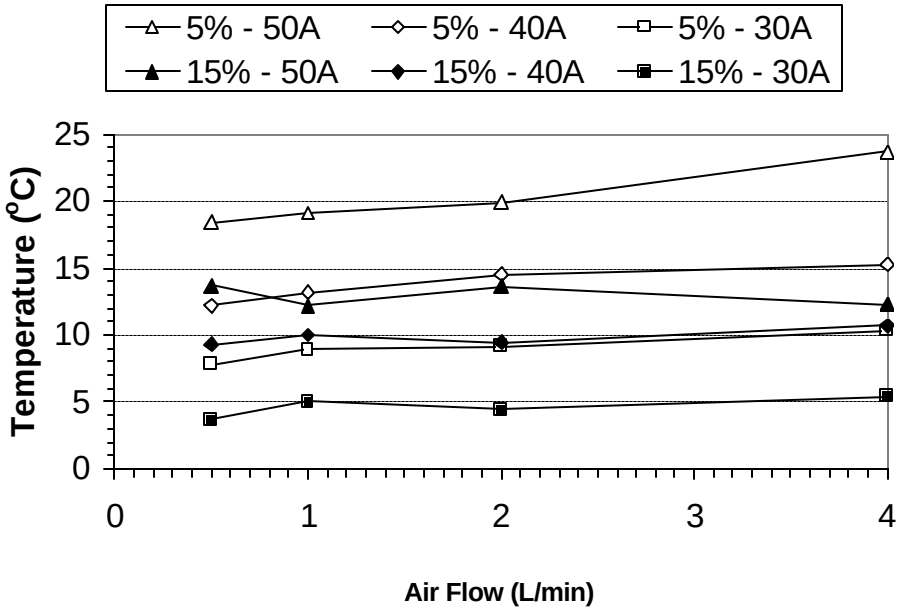

Figure 5.6. Temperature rise of 80ppi metal foam heaters after 20 minute heating time.

The results for 100 ppi foam are summarized in Fig. 5.7. The effect of relative density on temperature rise is most obvious from these results. It is noted that the 5 wt% foam has a higher temperature rise at 40 A than the 15 wt% foam has at 50 A.

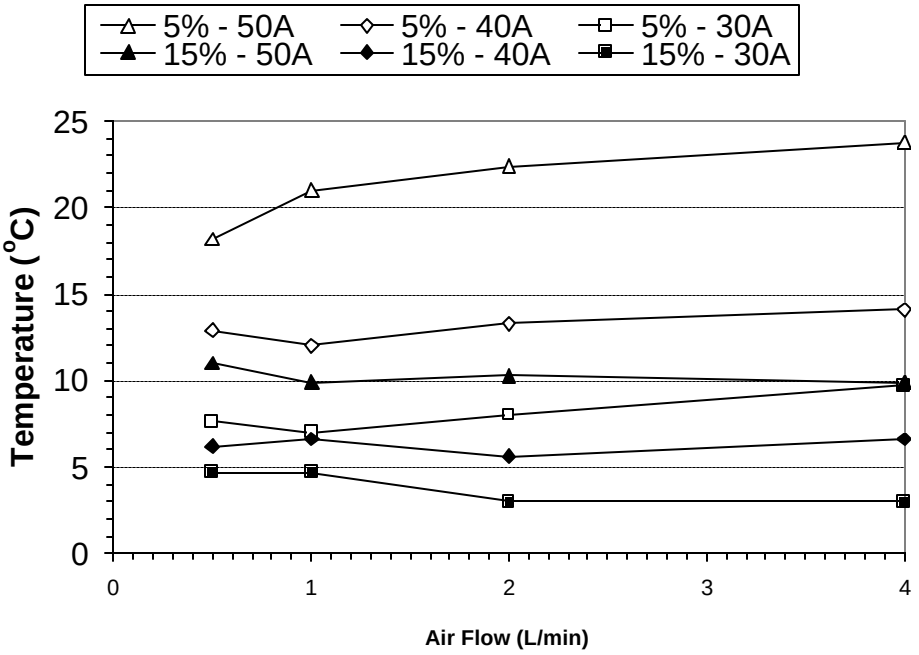

Figure 5.7. Temperature rise of 100ppi metal foam heaters after 20 minute heating time.

The effect of electrical current on outlet temperature is as expected; when more electrical current is supplied to the metal foam heater, more heat is generated, and temperature rise is higher. The effect of the air flow rate on temperature rise is not as obvious. As the air flow rate increases, the residence time of the air through the heater is likewise decreased, leading to lower outlet temperatures. At the same time, however, the convective heat transfer coefficient increases, leading to more heat gain and higher temperatures. Balance of the short residence time and high thermal convection can be seen in Figs. 5.5 through 5.7. It appears that for the 15 wt% heaters, the residence time effect is dominant. That is, at higher flow rates, the air has less time to pick up thermal energy and leaves the heating element at a lower temperature than it does at low flow rates. This effect is most obviously illustrated by the 60 ppi foams in Fig 5.5. The opposite seems to be the

case for the 5 wt% foams. For these foams, more heat is available to the air, and the increased effectiveness of the convective heat transfer due to higher flow rates causes the air to leave at a higher temperature than it does at lower flow rates. This effect of air flow rate on temperature rise is most obvious for the 5 wt% foam at 50 A shown above in Fig. 5.7.

5.2.3. Effects of Relative Density and Porosity

The effect of the weight density of the metal foam on the temperature rise is obvious. As shown in Fig. 2.2 and Table 2.1, higher wt% foam has more metal and lower electrical resistivity. During electrical heating, less heat is generated and the temperature rise is lower. Figs. 5.5 through 5.7 indicate that 15 wt% metal foam heaters generate significantly less temperature rise than the 5 wt% metal foam heaters under the same testing conditions. The interplay between the weight density effects, and the airflow rate effects was not expected, and needs more testing to quantify thoroughly.

The porosity of the metal foam changes the electrical resistivity and the temperature rise. There is no clear trend relating resistivity and porosity. The 80 ppi foams, as shown in Table 2.1 have the highest resistivity, and therefore, the highest temperature rises for otherwise identical test conditions. All the foams were made from the same batch of metal powder and fired at the same time. These differences could be due to variations in the manufacturing process, but samples from different batches of powder and different firings need to be examined to be sure.

5.3. Comparison of Experimental and Numerical Analyses

Since the FLUENT models predict the steady-state equilibrium temperatures, they must be compared to a steady-state experimental result to have any meaning. The only

experiment to truly reach steady-state is the 5 hour long-duration test. The maximum measured temperature rise for this test is 33. The FLUENT model predicts a mass-weighted average temperature rise of 40 ^{o}C. At least for the conditions tested, the FLUENT model and the experimental results agree quite well.

6. Concluding Remarks

In this study, a novel metal foam heater is examined. Five prototype metal foam heaters made of 60, 80, and 100 ppi Fe-Cr-Al foam at 5 and 15 wt% were tested. There was no 60ppi 5 wt% heater. Temperature rise of a metal foam heater for extended period of time is studied to understand the time to reach steady-state heat transfer condition. Experiments were conducted using the five heaters at four levels of air flow rate and three levels of electrical current to investigate the temperature rise of the air flow through the metal foam. The computational fluid dynamics modeling of the metal foam heater using FLUENT showed good agreement with the experimental steady-state temperature rise in the outlet of the 100 ppi, 5 wt% metal foam heater under 50 A electrical current and 5 L/min air flow rate.

It is possible to increase the resistance of the heating element by reducing its thickness. If thickness is decreased with increasing radius, a more uniform heat generation rate will result. This part could be produced from constant thickness metal foam using a cylindrical wire EDM process [Qu et al., 2001]. The variable thickness design is illustrated in Fig. 6.1.

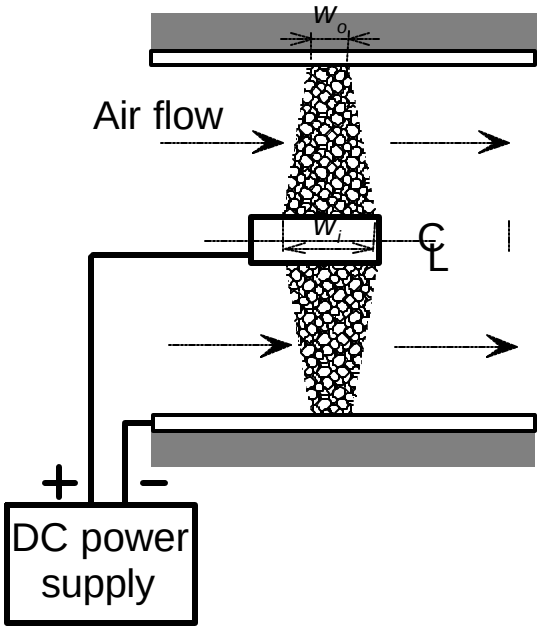

Figure 6.1. The cross-section of a variable thickness metal foam heating element.

Reducing the width of the metal foam will increase the electrical resistance and raise the temperature of the metal foam. However, under a constant flow rate, residence time of the air in the foam is shortened. This could possibly reduce the heat transferred to the air.

It also may be possible to increase the power output by the heater by passing the electrical current through several heating elements in series. Since one individual heater consumes approximately 6W of electrical power, when running at 50A, the 1000W DC power supply used during testing could power a heater with about 160 elements. One possible multi-element configuration is shown in Figure 6.2. In this configuration, each element receives preheated air from stage before it.

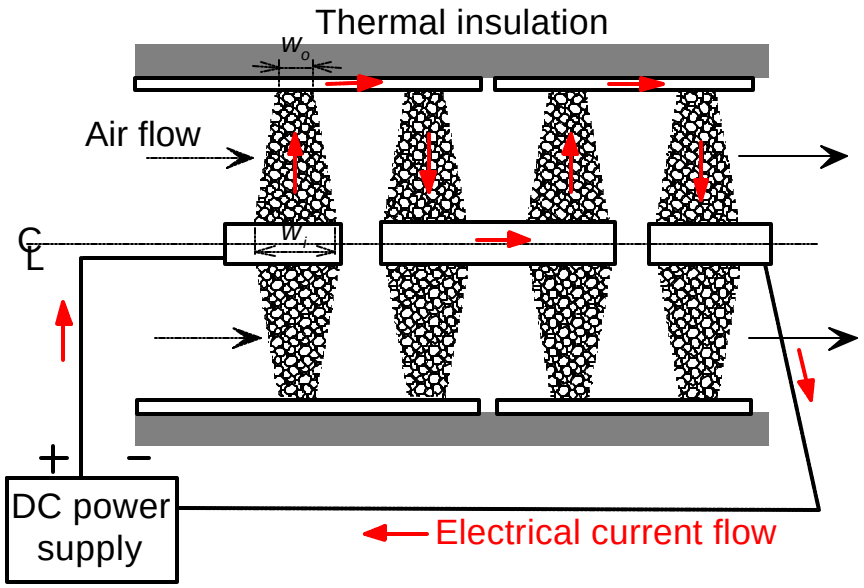

Figure 6.2. Multi-stage heater with elements connected in series.

References

Ashby, M., Fleck, N.A., Hutchinson, J.W., Gibson, L.J., Wadley, H., Evans, A.G., Wadley, H.N., 2000, *Metal Foams - A Design Guide*, Butterworth-Heinemann.

Banhart, J., 2001, "Manufacture, Characterization and Application of Cellular Metals and Metal Foams," *Progress in Material Science*, Vol. 46, pp. 559-632.

Blacker, T., 1996, "The Cooper Tool," *5th International Meshing Roundtable*, Sandia National Laboratories, pp 13-30.

Erickson, C. J., 1995, *Handbook of Electrical Heating for Industry*, IEEE Press.

Floyd, D., 2001, *Fluid Properties of Open Cell Sintered Iron Based Porous Metal Structures, Experimental Results and Discussion*, Porvair Fuel Cell Technical Report.

Hegbom, T., 1997, *Integrating Electrical Heating Elements in Appliance Design*, Marcel Dekker, New York.

Incropera, F., Dewitt, D., 2002, *Introduction to Heat Transfer*, Wiley, New York.

Kanthal, 2001, *Kanthal Handbook – Heating Alloys for Electric Household Appliances*, Kanthal AB.

Lu, T. J., Stone, H. A., Ashby, M. F., 1998, "Heat Transfer in Open-Cell Metal Foams," *Acta Materialia*, Vol. 36, pp. 3619-3635.

Qu, J., Shih, A. J., and Scattergood, R. O., 2002, "Development of the Cylindrical Wire Electrical Discharge Machining Process: Part I: Concept, Design, and Material Removal Rate," *ASME Journal of Manufacturing Science and Engineering*, Vol. 124, No. 3, pp. 702-707.

Yoro, K., Itsauaki, S., Saito, H., Nakajima, S., and Okamoto, S., 1998, "Diesel Particulate Filter Made of Porous Metal", *Diesel Exhaust Aftertreatment*, SAE Special Publications, Vol. 1313, SAE Paper # 980187, pp. 17-23, SAE, Warrendale, PA.

Appendix A. Tabulated Temperature Data for Short Duration Tests

Table A.1. Maximum Measured Temperatuers in 60 ppi, 15 wt% heater near Steady State.

60 ppi, 15% Density – Temps Listed (Inlet/Outlet/Ambient) in ^{o}C				
Current \ Flow	0.5 L/min	1.0 L/min	2.0 L/min	4.0 L/min
30A	26.3 / 30.4 / 25.5	25.3 / 29.3 / 26.0	26.1 / 29.0 / 25.2	25.1 / 28.5 / 24.5
40A	25.4 / 33.1 / 26.0	26.6 / 32.9 / 25.6	26.0 / 32.5 / 25.0	25.1 / 31.6 / 23.8
50A	28.6 / 38.6 / 27.5	32.3 / 36.2 / 26.8	31.2 / 35.4 / 26.1	28.2 / 34.2 / 24.8

Table A.2. Maximum Measured Temperatures in 80 ppi 5 wt% heater near Steady State.

80 ppi, 5% Density – Temps Listed (Inlet/Outlet/Ambient) in ^{o}C				
Current \ Flow	0.5 L/min	1.0 L/min	2.0 L/min	4.0 L/min
30A	29.0 / 36.4 / 28.6	28.9 / 36.9 / 28.0	30.0 / 38.1 / 29.0	30.3 / 39.0 / 28.7
40A	30.0 / 42.5 / 30.3	30.3 / 43.2 / 30.0	30.8 / 44.5 / 30.0	30.6 / 45.2 / 29.9
50A	29.3 / 47.0 / 28.6	41.0 / 49.0 / 29.9	40.8 / 49.6 / 29.7	37.3 / 53.1 / 29.4

Table A.3. Maximum Measured Temperatures in 80ppi 15 wt% heater near Steady State.

80 ppi, 15% Density – Temps Listed (Inlet/Outlet/Ambient) in ^{o}C				
Current \ Flow	0.5 L/min	1.0 L/min	2.0 L/min	4.0 L/min
30A	27.6 / 31.6 / 27.9	25.6 / 30.4 / 25.4	24.6 / 29.7 / 25.3	24.5 / 29.3 / 23.9
40A	30.9 / 38.8 / 29.3	29.9 / 38.5 / 28.5	29.4 / 38.0 / 28.6	29.3 / 37.7 / 27.0
50A	32.2 / 43.7 / 30.0	45.8 / 42.7 / 30.5	42.7 / 43.3 / 29.7	42.0 / 40.3 / 28.0

Table A.4. Maximum Measured Temperatures in 100 ppi 5 wt% heater near Steady State.

100 ppi, 5% Density – Temps Listed (Inlet/Outlet/Ambient) in ^{o}C				
Current \ Flow	0.5 L/min	1.0 L/min	2.0 L/min	4.0 L/min
30A	23.9 / 31.2 / 23.6	32.1 / 39.2 / 32.2	33.2 / 40.6 / 32.6	22.4 / 31.1 / 21.4
40A	26.4 / 39.7 / 26.8	29.7 / 41.9 / 29.9	28.9 / 41.3 / 28.0	26.6 / 40.2 / 26.1
50A	28.6 / 47.7 / 29.5	42.8 / 52.0 / 31.0	39.6 / 52.9 / 30.5	40.2 / 54.1 / 30.3

Table A.5. Maximum Measured Temperatures in 100 ppi 15 wt% heater near Steady State.

100 ppi, 15% Density – Temps Listed (Inlet/Outlet/Ambient) in ^{o}C				
Current \ Flow	0.5 L/min	1.0 L/min	2.0 L/min	4.0 L/min
30A	31.5 / 35.3 / 30.6	32.6 / 36.0 / 31.3	33.0 / 35.8 / 32.8	32.5 / 35.0 / 32.0
40A	31.0 / 37.7 / 31.5	31.7 / 37.9 / 31.3	29.8 / 35.3 / 29.7	29.0 / 34.3 / 27.7
50A	31.1 / 41.2 / 30.2	32.6 / 36.7 / 26.8	33.8 / 38.4 / 28.1	35.1 / 39.2 / 29.3

Appendix B. More Detailed SEM Micrographs of Fe-Cr-Al Foams

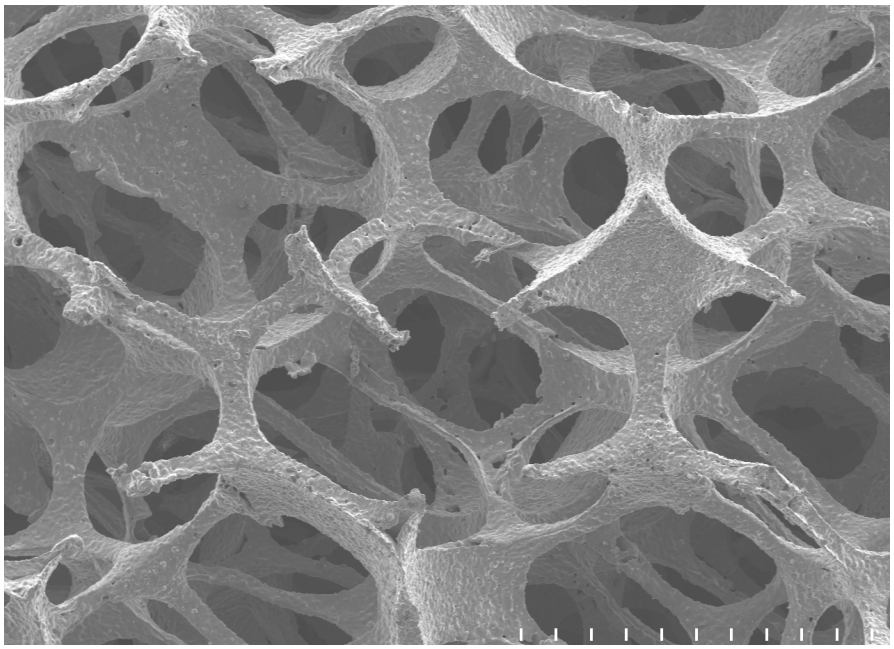

Figure B.1. SEM image of 60 ppi 5 wt% Fe-Cr-Al.

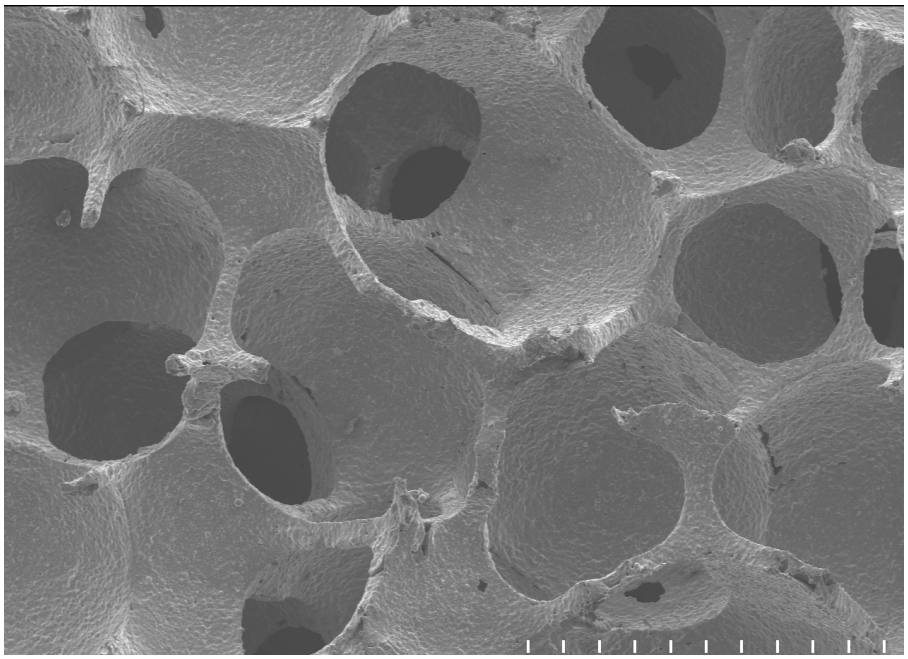

Figure B.2. SEM image of 60 ppi 15 wt% Fe-Cr-Al.

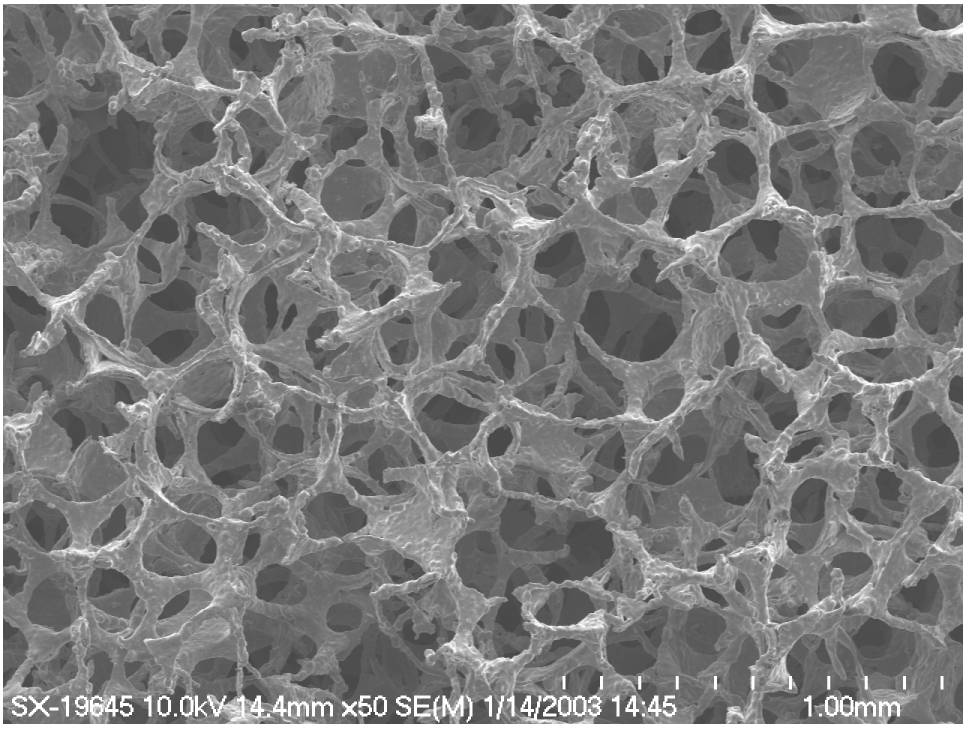

Figure B.3. SEM image of 80 ppi 5 wt% Fe-Cr-Al.

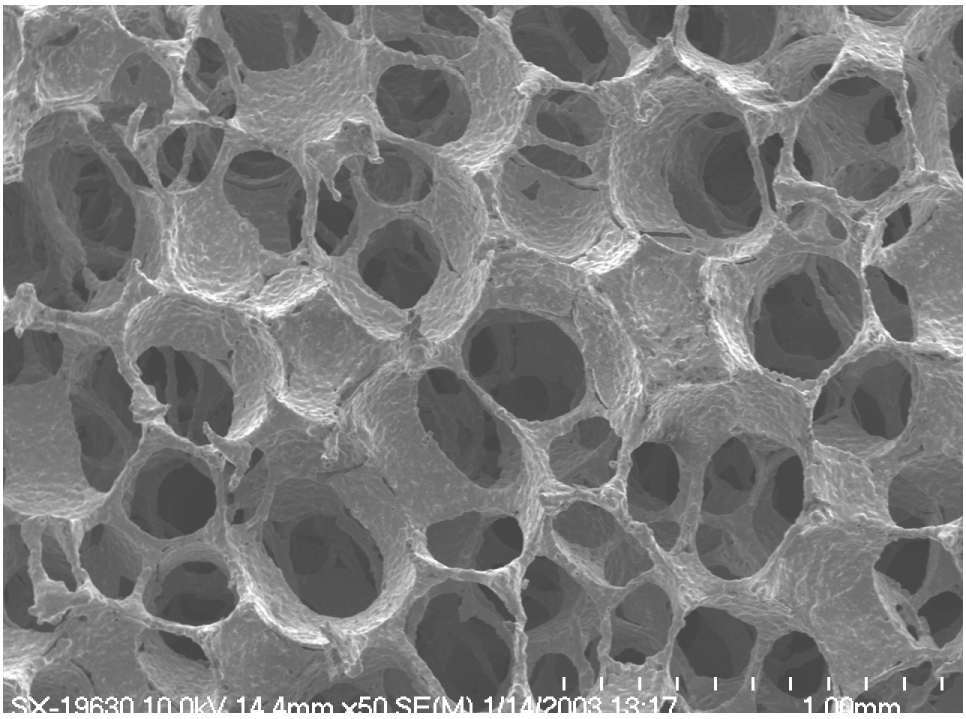

Figure B.4. SEM image of 80 ppi 15 wt% Fe-Cr-Al.

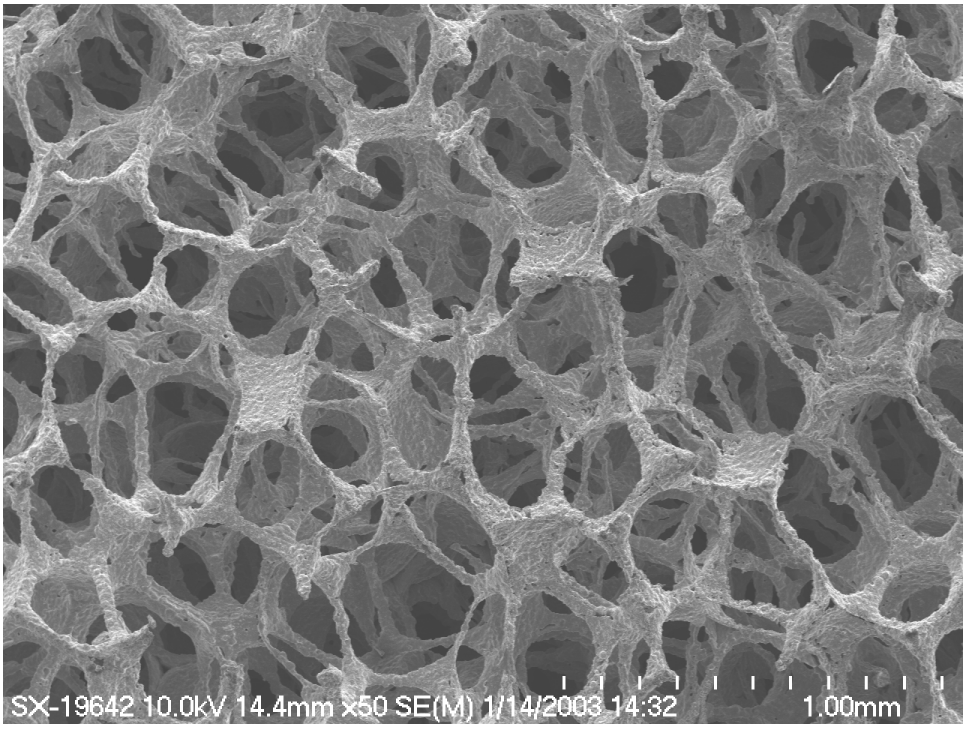

Figure B.5. SEM image of 100 ppi 5 wt% Fe-Cr-Al.

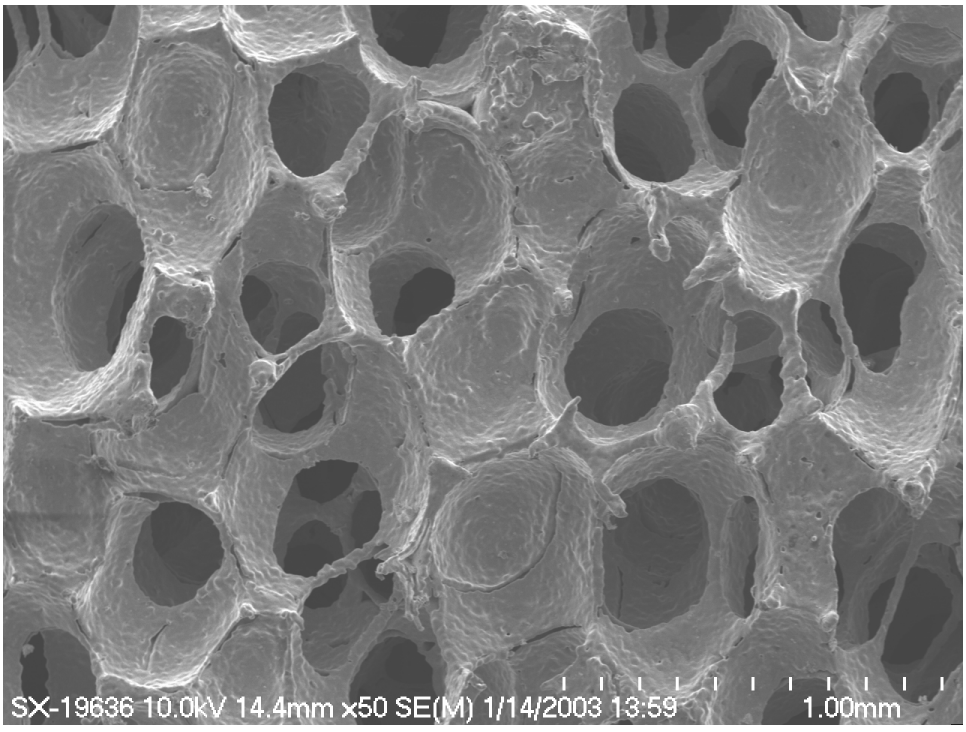

Figure B.6. SEM image of 100 ppi 15 wt% Fe-Cr-Al.